CLEEN
Cluster for Energy and Environment

Research Report
Helsinki 2012

Tähtinen Matti

Report: Studies of CLC hydrodynamics and test rig design

ccsp
Carbon Capture and Storage Program

CLEEN LTD
ETELÄRANTA 10
P.O. BOX 10
FI-00130 HELSINKI
FINLAND
www.cleen.fi

Cleen Ltd.
Research Report

Tähtinen Matti

Report: Studies of CLC hydrodynamics and test rig design

ccsp
Carbon Capture and Storage Program

Cleen Ltd
Helsinki 2012

Report Title: Studies of CLC hydrodynamics and test rig design

Key words:

Chemical looping combustion, hydrodynamics, scaling, cold model, double exit loop-seal

Abstract

This paper reports the results of tests of hydrodynamics and fluidization at chemical looping combustion, cold model scaling and built cold model of two interconnected fluidized beds.

The study was aimed to determine if it is possible to handle stable fluidization and solid circulation in the two interconnected fluidized beds with two double loop-seals. The tests and study show that it indeed is possible, using the cold model which was designed and built in the present work.

Helsinki, November 2012

Table of contents

1 Introduction

A reactor system has been constructed for hydrodynamic testing, especially designed for chemical looping combustion (CLC) testing. The system includes two circulating fluidized beds and two double exit loop-seals. Fluidization and hydrodynamics, which are essential parts of the operation, can be studied with the present reactor configuration.

Knowledge of hydrodynamics and solid circulation is needed to design and build reactor system which can be used to study CLC reactions at hot conditions. Without this knowledge possibility of faulty design increases and operation of process may be dangerous.

The report is divided into three parts. The first part explains the basics of fluidization and the second part introduces the cold model design. The third part shows how these things are implanted to the current cold model and results of tests.

2 Fluidization

Fluidization is a process where gas or liquid is brought into contact with solid particles in order to form a fluid-like state. Usually fluidization is performed with gas which is fed from below so that the solid particles are in constant motion with the gas stream. (Kunii & Levenspiel, 1977)

Fluidization is usually divided by fluidization conditions in five different groups: spouted bed, bubbling bed, turbulent fluidization, fast fluidization and pneumatic conveying. The fluidization regions are not exact and overlap usually with each other.

Spouted bed operates at the spouting bed region where the minimum fluidization velocity, U_{mf}, is not exceeded. Bubbling fluidized bed (BFB) operates on the bubbling bed region and usually does not exceed the terminal velocity of the particles, U_t. Circulating fluidized bed (CFB) operates at the turbulent region of fluidization, between the bubbling bed and fast fluidization regimes. Characteristic velocities of fluidization cannot be unambiguously presented because of the wide span of the particle size distribution (PSD) in the process. Dense circulating fluidized bed (DCFB) operates at same region, but voidage, ϵ, is higher.

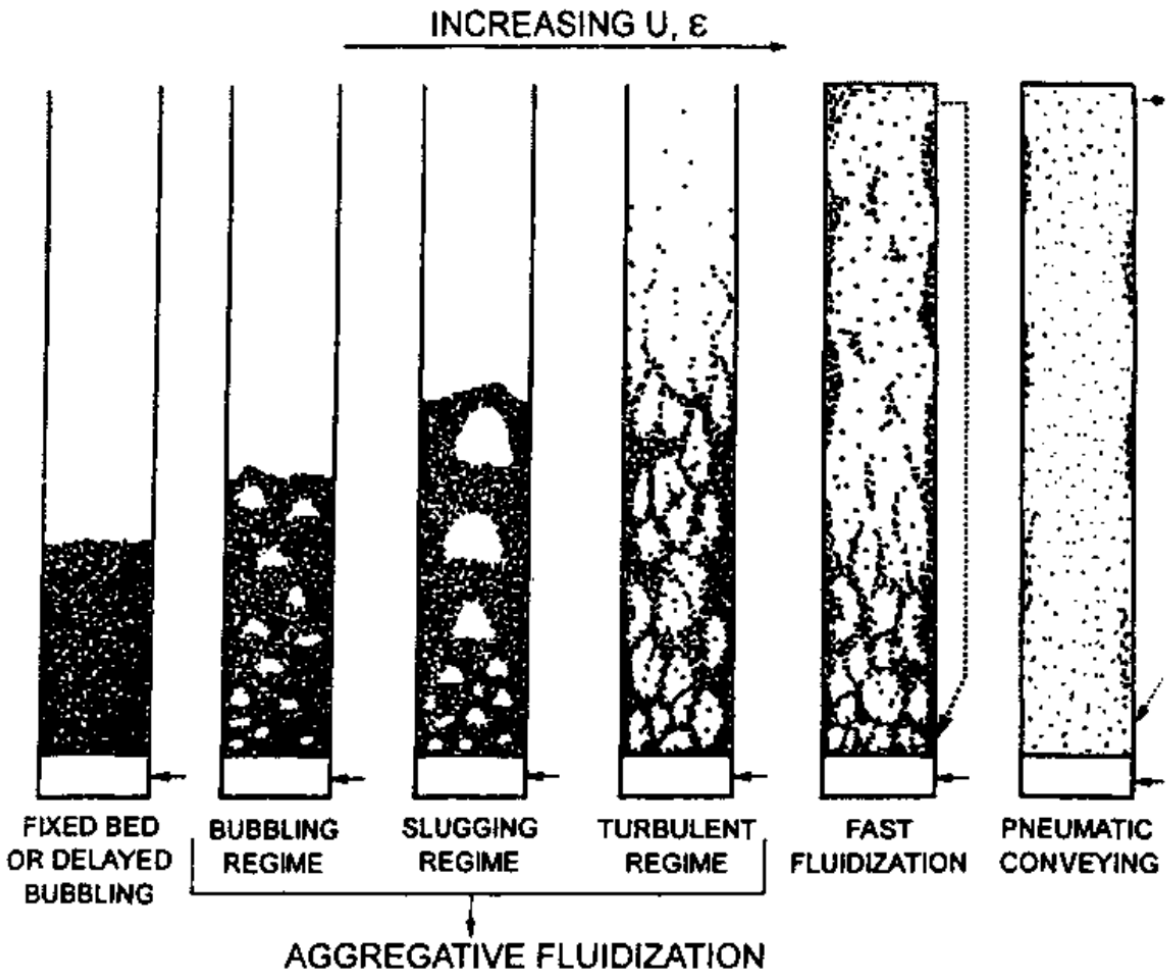

Fig. 1 Different fluidization flowtypes (Grace, 1986)

The different fluidization conditions are presented in Fig. 1. In combustion processes, usually the bubbling regime and fast fluidization are used.

Fig. 2 presents a regime map of operational regions of gas-solid fluidized beds. The map is divided in different regimes by particle size and fluidization velocity. When the fluidization velocity increases or the particle dimension decreases, the fluidization process becomes more rapid. The particle size is also divided in five different classes (Geldart, 1973).

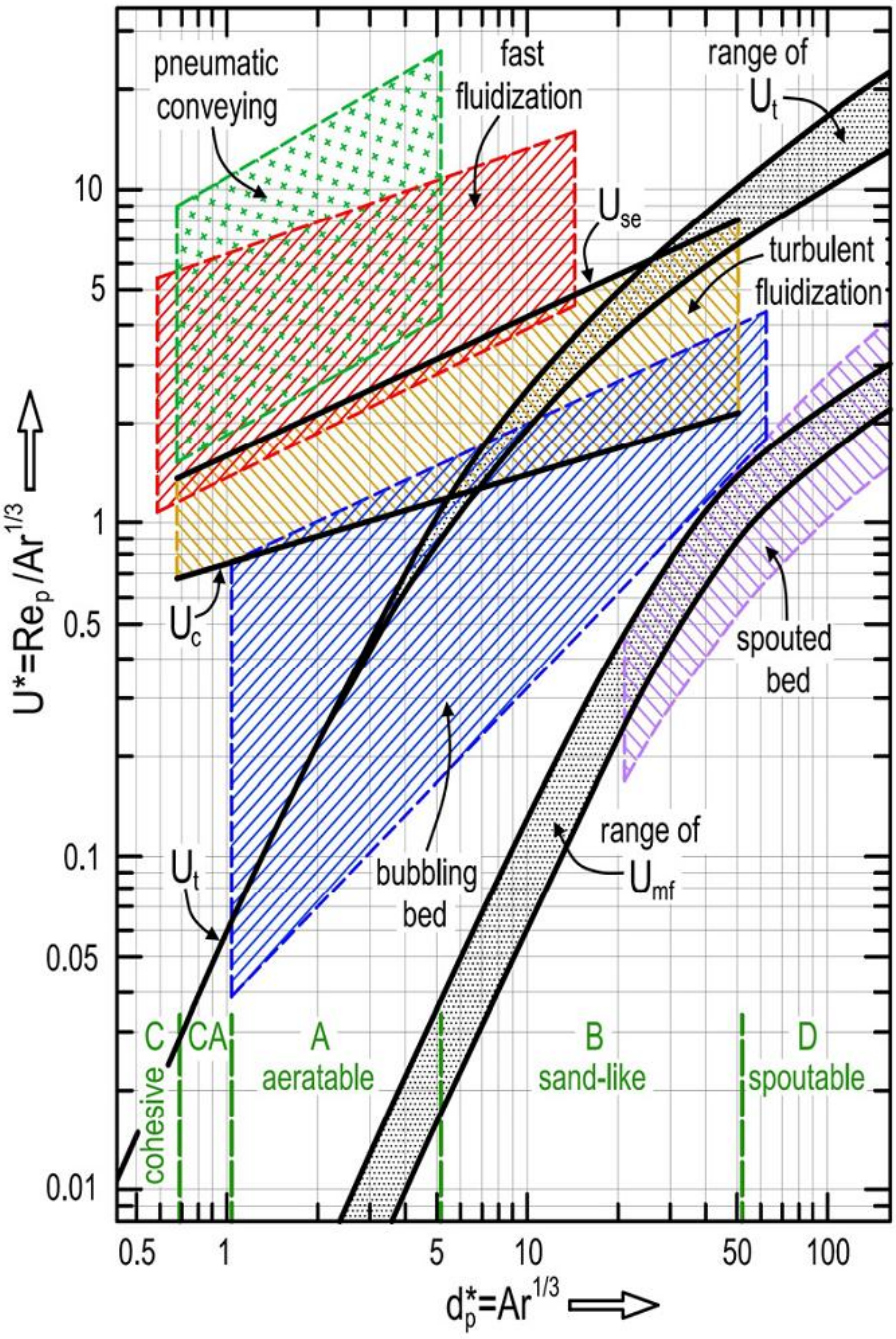

Fig. 2 Generalized regime map of gas–solid fluidized beds with typical operation regions of industrial reactors. Regime map combined from: Grace (1986), Ut(ϵ=0.8 to 1.0): Haider and Levenspiel (1989), U_c & U_{se}: Abba, Bi and Grace (2003) by (Schmid, et al., 2011)

2.1 Fluidization velocities

The fluidization process has a few reference velocities which divide fluidization into different regions. However, depending on the size and properties of the particles, all the velocities are not exact and well defined, which is not even needed.

The minimum fluidization velocity, U_{mf}, describes the velocity when the bed expands and becomes fluidized. The interactions of the particles change and they start to move (Raiko, et al., 2002). The minimum fluidization velocity can be approximated using Eq. 1, if the minimum fluidization voidage, ϵ_{mf}, is known. The minimum fluidization velocity can also be determined experimentally. (Kunii & Levenspiel, 1977)

$$\frac{1.75}{\phi_s \epsilon_{mf}^3}\left(\frac{d_p U_{mf}\rho_g}{\mu}\right)^2 + \frac{150(1-\epsilon_{mf})}{\phi_s^2 \epsilon_{mf}^3}\left(\frac{d_p U_{mf}\rho_g}{\mu}\right) = \frac{d_p^3 \rho_g (\rho_s - \rho_g) g}{\mu^2} \quad \text{Eq. 1}$$

The bed starts to expand when U_{mf} is exceeded for particles at Geldart Group A. Bubbles start to appear when the superficial velocity exceeds the minimum bubbling velocity, U_{mb}. As opposed to Geldart Group B and D particles, there is a delayed bubbling regime caused by interparticle forces. For Geldart Group B and D particles, U_{mf} and U_{mb} are usually defined as equal. Equation for this is obtained from experiments.

The onset velocity for turbulent fluidization, U_c, is the velocity when the amplitude of the fluctuation in the bed has reached its peak value. The fluctuation can be measured from pressure. The parameter U_c is the velocity when the transition from bubbling to turbulent bed starts. The transition starts from the top of the bed, proceeding towards the bottom.

When superficial velocity increases after onset velocity, fluctuation amplitude decreases and transition from bubbling to turbulent bed has taken place. This is called velocity of completion of transition to turbulent fluidization, U_k.

The terminal velocity, U_t, or free-fall velocity of particles, is the velocity when the entrainment of particles to the fluidization gas stream starts. The terminal velocity is presented in Eq. 2.

$$U_t = \left[\frac{4gd_p\,(\rho_s - \rho_g)}{3\rho_g C_d}\right]^2 \qquad \text{Eq. 2}$$

Transport velocity is the velocity when the bed changes from turbulent to fast fluidized. Usually this velocity is determined when particle clusters exceed the terminal/free fall velocity, U_t, This will rapidly increase particle entrainment from the bed.

The transport velocity, U_{tr}, can be determined using two different criteria, the solid concentration and entrainment of particles. The ways to detect these effects can vary. Fig. 3 presents an example of how the transport velocity is determined from the pressure gradient peak with increasing fluidization velocity. The transport velocity may be referred as critical velocity, when the entrainment of particles is used as detection criteria.

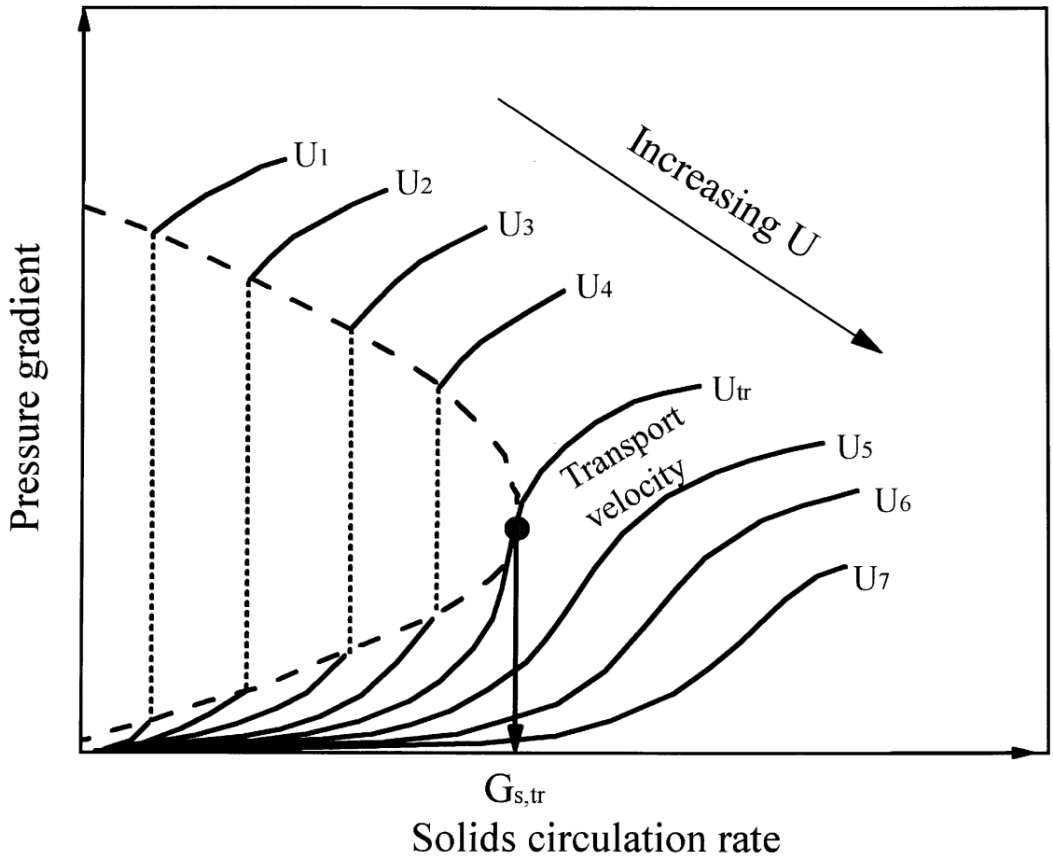

Fig. 3 Definition of transport velocity, by Yerushalmi and Cankurt (1979) at (Bi, et al., 2000)

The slip velocity, U_s, is the velocity difference between the solid and gas flows. The gas velocity approaches the slip velocity when the solid velocity goes to zero.

Table 1 summarises the different fluidization velocity ranges and regimes. Depending on the process conditions and particle properties of the system, all fluidization regimes may not be achievable.

Table 1. Summary description of Different Regimes of fluidization (Yang, 2003)

Velocity range	Fluidization regime	Fluidization features and appearance
$0 \leq U < U_{mf}$	Fixed bed	Particles are quiescent; gas flows through interstices
$U_{mf} \leq U < U_{mb}$	Particulate regime	Bed expands smoothly and homogeneously with small-scale particle motion; bed surface is well defined
$U_{mb} \leq U < U_{ms}$	Bubbling regime	Gas bubbles form above distributor, coalesce and grow; gas bubbles promote solids mixing during rise to surface and breakthrough
$U_{ms} \leq U < U_c$	Slug flow regime	Bubble size approaches bed cross section; bed surface rises and falls with regular frequency with corresponding pressure fluctuation
$U_c \leq U < U_k$	Transition to turbulent fluidization	Pressure fluctuations decrease gradually until turbulent fluidization regime is reached
$U_k \leq U < U_{tr}$	Turbulent regime	Small gas voids and particle clusters and streamers dart to and fro; bed surface is diffused and difficult to distinguish
$U > U_{tr}$	Fast fluidization	Particles are transported out of the bed and need to be replaced and recycled; normally has a dense phase region at bottom coexisting with a dilute phase region on top; no bed surface
$U \gg U_{tr}$	Pneumatic conveying	Usually a once-through operation; all particles fed are transported out in dilute phase with concentration varying along the column height; no bed surface

A deeper analysis of the fluidization velocities and measurement techniques is presented by (Bi, et al., 2000).

2.2 Particle size distribution

Studies indicate that the effect of particle size distribution (PSD) is important for fluidization systems. However, all the dependencies between particle size distribution and fluidization are not yet fully understood.

Usually in the fluidization process, the particle size distribution is continuously changing as fluidization material is added, composed and it breaks down during the process. As an example in the chemical looping process, a new oxygen carrier is added, it may bind impurities to compose new particles and the worn oxygen carrier may break down by abrasion or fragmentation.

The breakdown can occur either by abrasion or fragmentation. In abrasion, fines are grinded from the surface of particle while the size of the mother particle stays almost the same. In fragmentation, the mother particle breaks down to multiple smaller particles. The effect of these two processes on the PSD is different and can be seen in Fig. 4.

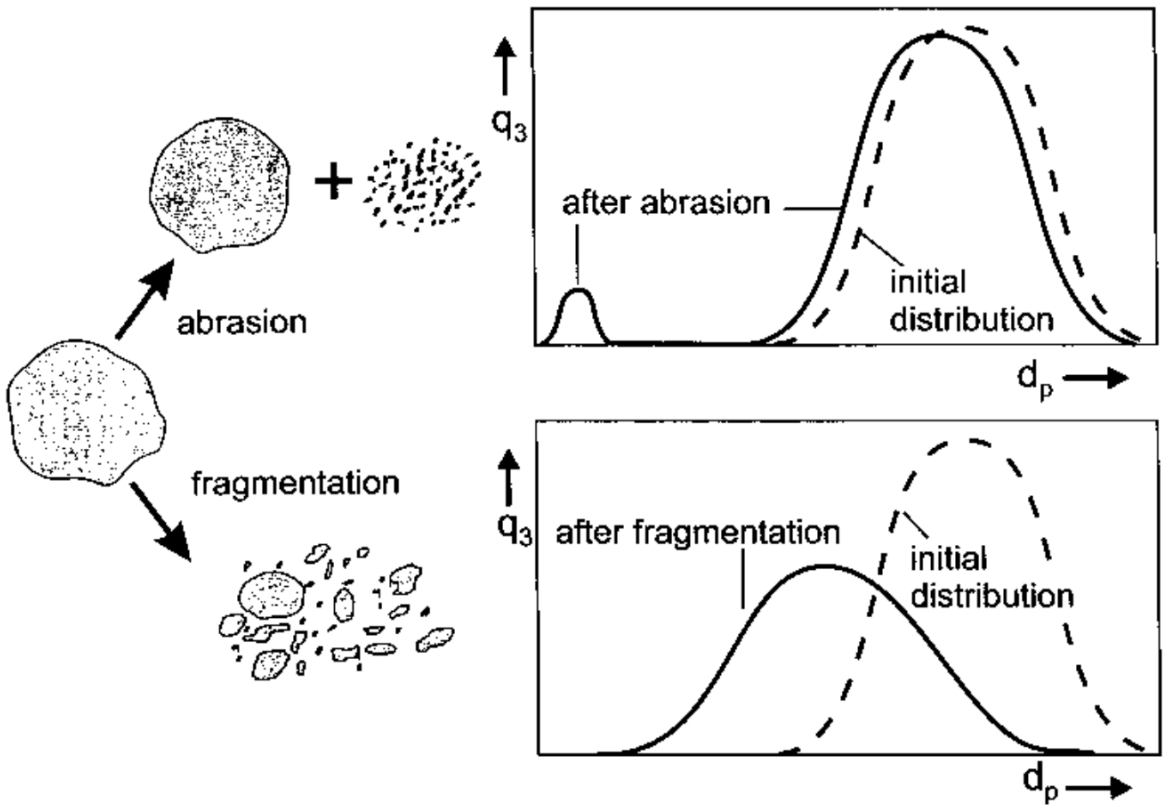

Fig. 4 Attrition as abrasion and fragmentation and effect to particle size distribution. (Yang, 2003)

For example for oxygen carriers, depending on particle properties, both abrasion and fragmentation are possible. Usually abrasion is connected to mechanical stress if collision velocities are not high and fragmentation may be caused by chemical and heat stress.

2.3 Entrainment and elutriation

Entrainment means the flux of particles which is carried out from the bed with the fluidization gas. Elutriation is defined as the change of particle distribution or classification in the bed, caused by entrainment of particles.

A fluidized bed is divided into different zones, usually dense bed and freeboard. An increase in the superficial velocity increases surface fluctuations and generates a clear difference between the two zones. When the surface fluctuations are high enough, this zone is called a splash zone where particle ejection to freeboard takes place.

The entrainment process contains three steps, firstly transportation from the bed to freeboard, then acceleration by uprising gas and finally entrainment to the gas flow. Transportation to freeboard is connected to

eruption of bubbles at the splash zone. When a bubble erupts, particles splash to freeboard. The particles will accelerate if the gas flow is high enough and finally follow the gas flow separately, or as a part of a cluster.

If the particle size distribution is wide enough, fluidization can cause particle separation so that finer particles will accumulate to the top of the bed and coarse particles to the bottom. The velocity of the gas flow may then exceed the fine particle terminal velocity and blow the fine distribution to freeboard.

Elutriation is usually presented as *elutriation rate constant* K^*_{ih}*, defined as the ratio of the instantaneous rate of removal of solids of size* d_{pi} *based on the cross-sectional area A to the fraction of the mass of the bed material with size* d_{pi}*.(Joachim Werther and Ernst-Ulrich Hartge; at* Yang, 2003)

Elutriation is affected by particle size distribution, superficial velocity, freeboard height, bed diameter, internals, temperature and pressure. There is no comprehensive model for elutriation in the literature due to the complexity of the fluid dynamics and wide range of fluidization conditions.

A more precise description of entrainment and elutriation has been presented by Yang (2003).

2.4 Pressure drop and suspension profile

In the fluidized process, a pressure drop occurs. This effect is a combination of hydrostatic pressure, friction of the wall and the acceleration effect. Usually the friction of the wall and acceleration are neglected, but this is not always the case.

Wall friction cannot be neglected if the diameter of the bed is smaller than 0.1m. If the ratio of the cross section area to the perimeter becomes too small, more particles are in contact with the wall, increasing friction losses. At a large scale, the friction forces can be neglected.

The acceleration effect is usually neglected if the solid circulation rate is below 200 kg/m^{2}s. Error from the acceleration effect is higher at the bottom part of the bed where major acceleration takes place.

The pressure drop can be measured as a pressure difference between different sections of the riser. When the wall friction and acceleration effects are neglected, the axial suspension profile, ρ, can be calculated from measured pressure differences, ΔP, as

$$\rho = \frac{\Delta P}{gh} \qquad \text{Eq. 3}$$

Experimentally, the pressure measurement taps should be located denser in areas where the pressure gradient is higher. This is the case at the bottom of the bed where the dense bed first changes to splash zone and then freeboard. This is crucial for attaining a good voidage profile.

The solid circulation rate, G_s, and superficial gas velocity, U_s, have an effect to the shape of the voidage profile. An increase in G_s and the bed mass increase the height of the solid holdup on every height, but also change the shape of the profile. Position of the curve at profile usually rises. The pressure and voidage profiles are influenced also by secondary gas inlets, baffles, riser exit, and particle and process properties.

3 Design of cold model

A cold model is usually constructed to increase knowledge of the process and characteristics of the process conditions. It can be also used to improve or solve existing problems of hot or bigger units. Understanding of scaling and hydrodynamics are needed for cold model design.

The point of view of the cold model design becomes different if the process, reactor connections or characteristics are new or unknown. Verification of the cold model cannot be done if the system is constructed to test a new reactor and process concept, since there is no existing hot or large scale reactor or process for comparison.

Benefits of the cold model, compared to hot unit as test rig, are cheaper construction and use, the possibility to observe hydrodynamics visually, and more versatile measurement possibilities. The cold model is also safer to use, risk management is always easier when the process does not contain hot conditions or chemical reactions. The same factors are

also disadvantages, as the results cannot be directly applied to hot conditions, or scaled up. However, some chemical phenomena and heat transfer coefficients may be resolved indirectly from mass transfer measurements and existing knowledge.

3.1 Design goals and Requirements

The design goal is simple, to outline a cold model for hydrodynamic testing of chemical looping reactor system. Hydrodynamic testing is needed to test the reactor system concept and increase understanding of the characteristics of the process. Building of a hot test rig for a non-existing process and new reactor concept would be highly risky.

The design of the cold model includes determination of the requirements and defining the limits. Rest of the process is iteration within the defined limits to meet the requirements.

The leading requirement for the cold model design was versatility and possibility to modify reactors, measurements and connections. This is tied to uncertainties from the non-existent process. If the cold model can be modified easily after increased knowledge, better end results can be achieved.

Some of the physical limits were set by the surrounding infrastructure. The maximum fluidization volume flow per reactor is 1000Nl/min, which is limited by the pneumatics equipment. Air was selected as fluidization gas to reduce operational costs and simplify the test procedure. Height of the cold model test rig should be less than 4 meters, which is limited by space reserved for system.

The required recirculation of solids was chosen to be handled with a double exit loop-seal which is adjustable by fluidization volume flow. Initial tests with this kind of loop-seal were done with a smaller cold model earlier in 2011.

3.2 Scaling

Scaling is a part of the design process which ensures similarity between the cold or smaller scale devices and the hot or larger scale systems. Main focus of scaling at the fluidization process is hydrodynamic

similarity, when scaling is done at cold conditions. Scaling of heat transfer and chemical reactions can be neglected at this point.

To ensure proper hydrodynamic scaling, the ratio of important forces at fluidization should be the same. In practice this means that reactors having a different scale are compared to each other by dimensionless ratios.

There are different sets of dimensionless parameters. One of the most well-known is composed by Glicksman (1984). Eq. 4 presents a simplified group of dimensionless parameters while a full set of scaling parameters is given in Eq. 5, the latter also including forces which act in a fluidized bed, see Table 2.

$$\frac{U_0^2}{gD}, \frac{\rho_s}{\rho_f}, \frac{U_0}{U_{mf}}, \frac{G_s}{\rho_s U_0}, \frac{L}{\mathrm{D}}, \phi, bed\ geometry, PSD \qquad \text{Eq. 4}$$

$$\frac{\rho_s U_0 d_p}{\mu}, \frac{\rho_s U_0 D}{\mu}, \frac{U_0^2}{gD}, \frac{\rho_s}{\rho_f}, \frac{G_s}{\rho_s U_0}, \frac{L}{\mathrm{D}}, \phi, bed\ geometry, PSD \qquad \text{Eq. 5}$$

The group of dimensionless parameters contains ratios and values which should be the same. To represent the scaled-up process well, the bed geometry should remain the same. In some cases, a simplified solution may be needed for example at the exit of the reactor, but these may influence the scalability.

The particle sphericity, Φ, should be same at both systems. The sphericity of particles is connected to fluidization by the Ergun equation which is used to determine the minimum fluidization velocity and packing of the bed. Keeping the same sphericity also ensures that the scaling of the PSD can be done.

The particle size distribution is very important part of the scaling. However, the distribution does not need to be exactly the same but rather so that the scaled PSD curves should be similar. In practice this means that the scaled particle diameter sets the position of the PSD curve, which should remain the same in the scaling. This can be seen

below where the particle inertia/gas viscous forces are examined at Table 2.

In chemical looping, a hot condition air reactor is fluidized by hot air to oxidize the oxygen carriers. The average temperature of the reactor was chosen to be 850°C for hot conditions and 25°C for cold conditions.

Table 2. Ratio of forces acting in a fluidized bed. (Yang, 2003)

$\rho_s U_0 d_p/\mu$	Particle inertia/gas viscous force
$\rho_f U_0 L/\mu$	Gas inertia/Gas viscous force
U_0^2/gL	Inertia/gravity force
ρ_s/ρ_f	Solid inertia/Gas inertia force
	Surface Forces—Collision, Adhesion; Form is Debatable
	Additional Important Ratios
$G_s/\rho_s U_0$	Solid recycle volumetric flow/Gas volumetric flow rate
L/D	Bed height/Bed diameter
PSD	Particle size distribution, χ_1 (mass fraction of d_i) for d_i/d_p (mean solid diameter) for all d_i's
φ	Particle sphericity

This gives the possibility to approximate the fluidized gas properties, namely density and viscosity. Ratio of the gas and solid properties can be calculated from the density. When using air as the fluidizing gas, the density of solids in the cold model can be solved from Eq. 6.

$$\left(\frac{\rho_f}{\rho_s}\right)_c = \left(\frac{\rho_f}{\rho_s}\right)_h \qquad \text{Eq. 6}$$

Combining the Reynolds number based on bed diameter and the square root of the Froude number, and rearranging, we obtain

$$\left(\frac{D_c}{D_h}\right) = \left(\frac{(\nu_f)_c}{(\nu_f)_h}\right)^{2/3} \qquad \text{Eq. 7}$$

This presents the optimal scaling ratio of geometry on defined fluidization gases and temperatures. If the scaling is done from 850°C air to 25°C, the change of density and viscosity set the optimal geometrical scaling ratio to be 4.43:1. However, when scaling from industrial scale to cold model, this scaling ratio is hard to keep.

The particle diameter, d_p be calculated using the Reynolds number ratio between the bed and particle diameters, which is simplified in Eq. 8.

$$\frac{\rho_f U_0 D}{\mu_f}\frac{\mu_f}{\rho_f U_0 d_p} = \left(\frac{D}{d_p}\right)_h = \left(\frac{D}{d_p}\right)_c \qquad \text{Eq. 8}$$

The similarity between Eq. 7 and Eq. 8 shows that the particle diameters follow the ratio of kinematic gas viscosities, v. The particle diameter can be scaled even if this does not reach the ratio between the bed diameters. Usually this means that at cold model consitions, the bed and particle ratio is higher than in the hot full scale unit.

To keep the hydrodynamic similarity in scaling, the Reynolds number and the Froude number should be same in both systems. By rearranging the Froude number, the superficial velocities can be matched between the systems.

$$\frac{U_{0c}}{U_{0h}} = \left(\frac{\nu_{fc}}{\nu_{fh}}\right)^{1/3} = \left(\frac{D_c}{D_h}\right)^{1/2} \qquad \text{Eq. 9}$$

It is important to notice that when the velocity scales depend on the kinematic viscosity in cube root, the ratio of time scales and frequencies depend on the kinematic viscosity at same ratio. This affects later the post-processing and scaling of the measurements.

To ensure that the solid concentration would be similar in both systems, Eq. 9 and the scaling parameter connected to volumetric solid recirculation and volumetric gas flow are combined in Eq. 10.

$$\frac{\left(\frac{G_s}{\rho_s}\right)_c}{\left(\frac{G_s}{\rho_s}\right)_h} = \left(\frac{\nu_{fc}}{\nu_{fh}}\right)^{1/3} \Rightarrow \frac{G_{sc}}{G_{sh}} = \left(\frac{\rho_{sc}}{\rho_{sh}}\right)\left(\frac{U_{0c}}{U_{0h}}\right) \qquad \text{Eq. 10}$$

3.3 Design

Scaling in practice means compromising between reality and making reasonable sacrifices on dimensional parameters. Ideal values for different parameters can easily be calculated while it is more difficult are to find reasonable design solutions so that these values could be met.

When the temperature of the process defines the gas properties, the deal solid density ratio can be calculated. Ideal ratios from earlier equations are presented in Table 3.

Table 3. Ideal ratios from dimensional parameters for cold model.

	Hot	**Cold**
Temperature	850	25
Dynamic gas viscosity, calculated	4,40E-05	1,86E-05
Gas density, calculated	0,32	1,20
Derived from scaling laws		
Solid density	ρ_s	3,75 ρ_s
Dimension, length, geometry	D	0,23 D
Particle diameter, sauter	d_p	0,23 d_p
Superficial velocity	U_0	0,48 U_0
Solid circulation	(Gs/ρ_s)	0,48 (Gs/ρ_s)
Time	t_h	0,48 t_c
Frequency	f_h	2,07 f_c

In hot conditions, the oxygen carrier apparent density varies at least from 800 to 4500 kg/m^3 (Johansson, 2007). For simplicity, it is assumed that the voidage at minimum fluidization, ϵ_{mf}, conditions at both reactors and particle sizes are the same, 0.46. The solid density of the oxygen carrier then varies from 1740 to 9780 kg/m^3. It is clear that it is hard to find a fluidization material for the cold model which is 3.75 times denser, cheap and non-toxic.

The fluidization particle material was chosen to be bronze which has quite a high density, is durable and easy to attain. The toxicity hazards of bronze are the same as for any very fine powder; breathing of dust or fume should be eluded. In the test, two different types of bronze particles were obtained.

Depending on the size of the CFB process, the length-to-width ratio varies from the commercial scale of 4:1 to the lab scale of 40:1, or even 80:1 (Johansson, et al., 2007). These ratios can be compared to the maximum height of the riser of 3.5 meters when the total height of the test rig would be nearly 4 meters. This comparison to the cold model gives a diameter from 0.044 to 0.875 meters.

When the riser diameter increases, the volume flow of the fluidization gas has to increase to maintain the same superficial velocity. Usually the superficial velocity is 2-5 times the terminal velocity in the CFB process.

This limits the riser diameter if the maximum fluidization volume flow is determined. In this case the flow is limited to 1000Nl/min and limit of the diameter is then 108mm at a superficial velocity of 2m/s.

The test rig configuration starts to take shape within these limits with the scaling parameters. Set of three different riser units was designed to increase versatility. The riser diameters were calculated and final diameters were chosen from standard pipe diameters. The final inner diameters of the risers are 40/69/104mm. The riser height can be adjusted between 500/1500/2500/3500mm. Table 4 presents how these dimension selections scale back to hot conditions.

Table 4. Scaled values from the cold model to hot conditions.

	Cold	**Hot**
Temperature	25	850
Riser dimension, D, meter	0,040	0,177
Three different risers	0,069	0,305
	0,104	0,460
Height of riser, meter	0,500	2,2
Adjustable on steps	1,500	6,6
	2,500	11,1
	3,500	15,5
Solid density, kg/m^3	8800	2387
Particle diameter, sauter, µm	45	265
Max superficial velocity at 1000 Nl/min	14,5	30,5
at riser dimensions 40/69/104mm	4,9	10,2
	2,1	4,5

Riser scales to hot conditions at range of pilot and demo scale. The hydrodynamic similarity during the tests is adjusted with superficial gas velocity under maximum fluidization volume flow and solid inventory.

All the distribution plates of the test rig are changeable which makes it possible to test different kind of configurations and fluidization possibilities. The plates are designed to produce even fluidization. This is achieved by making the plates so that they have an evenly distributed open area which is independent of the riser position to plate, shape or size. Material of the distribution plate was chosen to be steel.

The recirculation process is designed so that alternative non-mechanical valves can be tested. The junction interface after the cyclone and before the riser connection is flexible plastic tubing which makes it possible to connect any kind of recirculation system to the test rig.

In a circulating fluidized bed, the solid recirculation is handled usually with non-mechanical valves. In this case, the recirculation is handled with two double exit loop-seals which are controlled with the fluidization volume flow. The double exit loop-seal can be seen in Fig. 5**.**

The loop-seal is divided into three chambers; each of which is 30mm wide. Also the grate is divided into three sections of 30mm; fluidization of these sections can be separately adjusted. The total area of the grate is 9000mm^2.

The lengths of these chambers are 90mm and the height to the edge is 60mm. Space between the edge and the loop-seal ceiling is 30mm.

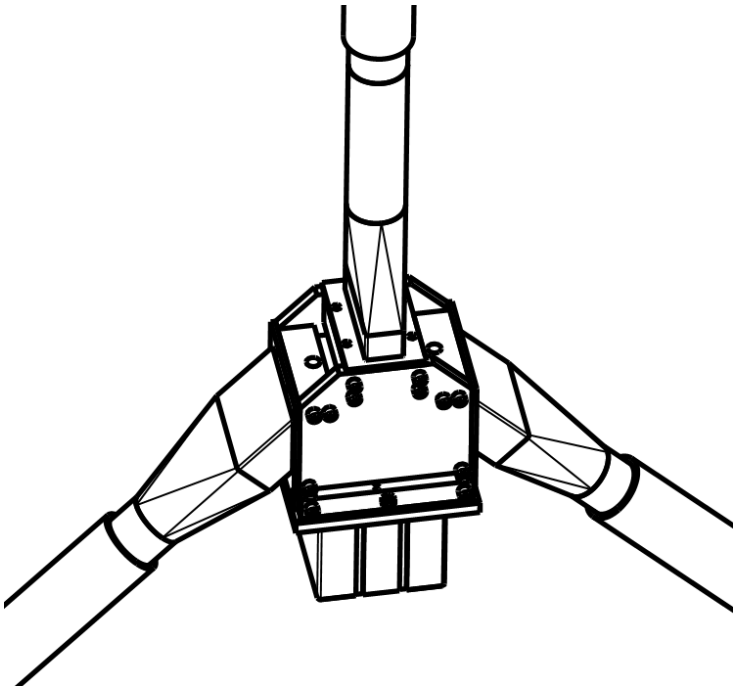

Fig. 5 Double exit loop-seal with separated air plenums. Connections from cyclone and to risers with couplings.

Both risers have two separated cyclones which are dimensioned to separate whole particle-size distribution. The primary cyclone is designed to separate major part of the solids at a higher solid circulation rate. The secondary cyclone is designed to separate fines from the gas flow. After the second cyclone, there is a pressure adjustable air amplifier to adjust pressure in the system. The cyclone setup is presented in Fig. 6.

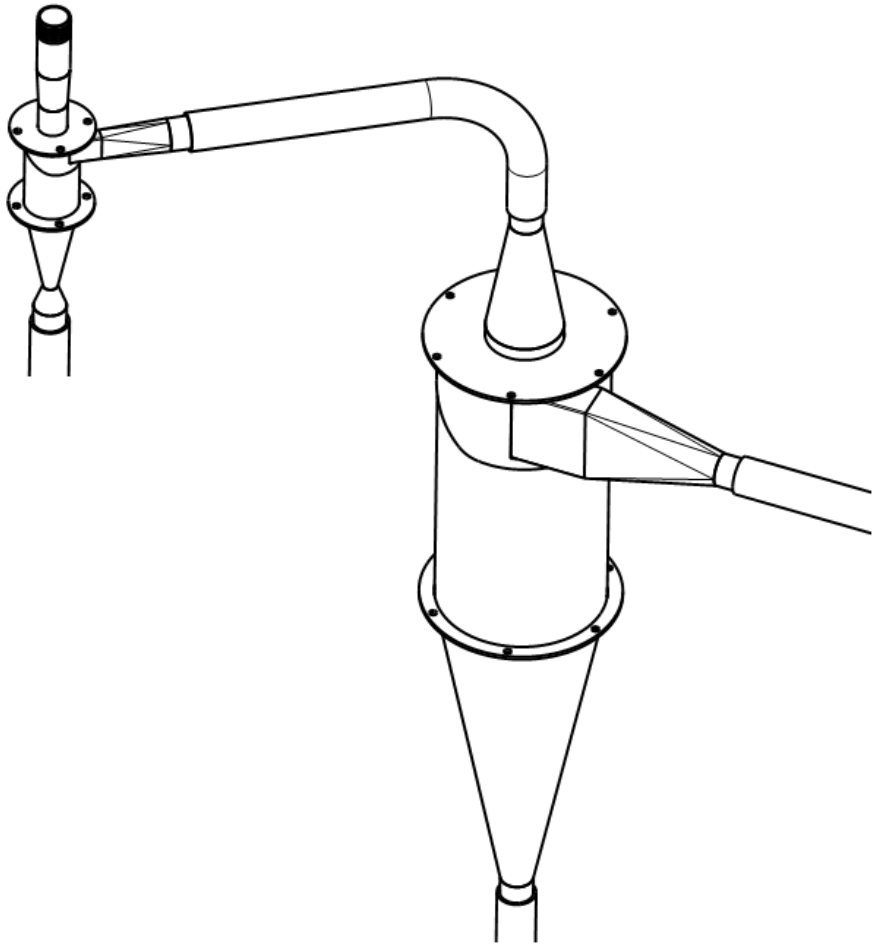

Fig. 6 Cyclone setup of one riser.

3.4 Construction and materials

The lowest parts of the riser are made from steel. At the bottom of the riser are an air plenum and the distribution plate. The air plenum and the lowest part of riser support the weight of the upper parts of the riser. The air plenum and lower part are connected with a sealed flange. The flange connection seals the distribution plate between the air plenum and the riser.

The three upper parts of the riser are made from acryl (polymethyl methacrylate, PMMA). The parts are connected to each other by flanges. These flange connections provide the possibility to add separated parts, such as baffles, to the riser for various measurements and the ability to adjust the custom height. The riser has a connection to the rig frame to support it vertically.

The loop-seals are constructed from acryl and steel. Acryl is chosen for material because it is clear and can be milled. The thickness of the plates is 10mm. The steel parts are precision milled or laser cut and used to support and maintain dimensions when the loop-seal is fluidized. The steel parts are connected to acryl by bolts and sealing is carried out by glue or liner.

The cyclones are constructed from acryl and steel. The bottom cone and the upper part of the cyclone, including connections, are made from steel. The upper part and the input connection are made so that mechanical stress from solid to acryl is reduced.

The middle part is made from acryl to maintain a good visibility into the cyclone. This makes it possible to inspect, visually and optically, the performance of the cyclones. It is also possible to change the middle part of the cyclone, if the acryl becomes dim or a different configuration of cyclones is wanted. The cyclone is assembled using glue and threaded rods.

The connections between these parts are made with dim plastic tubing. Even if the tubing is dim, it is possible to see the movement of the solid.

The fluidization gas flow is controlled by Bronkhorst mass flow meters. The maximum gas flow in both risers is 1000Nl/min. Both recycle chambers have a maximum gas flow of 100Nl/min at double exit loop-seals.

4 Test rig design

The test rig was constructed for versatile research connected to hydrodynamics. Possibilities to change the riser combination and connections are wide, only changing the diameters and lengths of the risers provides several different configurations.

For a commissioning test, it was chosen to use one set-up and carry out pressure difference measurements.

4.1 Set-up

The commissioning test used 40mm and 69mm risers at the length of 3500mm. The risers use only primary fluidization from the distribution plate, secondary gas inlet is not used. Both cyclones are used and

pressure is controlled by air amplifiers. Double exit loop-seals are used for recirculation valves.

The primary and secondary cyclones are in pairs at top section of test rig, as shown in Fig. 7. From the cyclones, the fluidization gas is directed to a bag filter at the upper working platform.

Fig. 7 Cyclones at the top of test rig. Primary cyclones are at the middle and secondary cyclones are on the edge of picture. Black tubes from secondary cyclones are connected to bag filter.

The double exit loop-seal is presented in Fig. 8. The picture shows that the loop-seal can be inspected from both sides. The gas distributor is divided into three sections. Sections under the recycling chambers are now open and the middle supply section is blind.

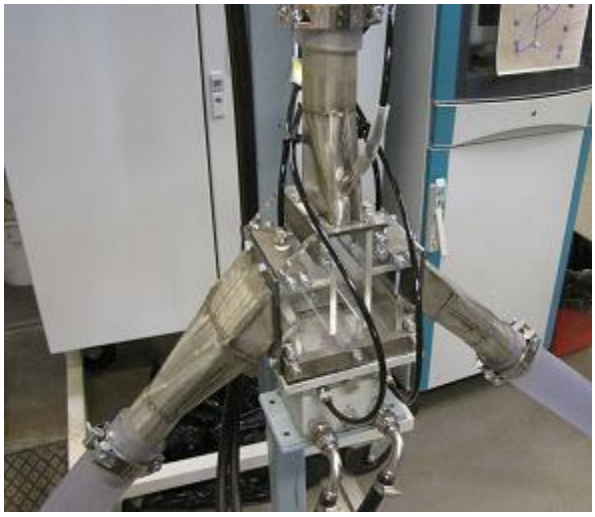

Fig. 8 Double exit loop-seal which is connected to reactors.

This setup was chosen because of its ability to test most of the possible and most wanted hydrodynamic subjects.

4.2 Measurements

The test rig contains multiple connection taps for pressure measurements, though all of them are not constantly used. The test rig has 32 pressure difference transmitters with selectable measurement range from HK instruments Oy.

The space between the possible measurement taps at the bottom of the riser section is 100mm. In the acrylic parts, the space is increased to 250mm. The pressure change gradient is higher at the bottom of the riser and more accurate pressure difference measurements are needed. All the riser section pressure taps are at 45 degree to decrease blockage. The diameter of the pressure taps is 6mm.

The measurement data is saved to a data logger at a rate of 5Hz. The fluidization volume flow control is logged to the data acquisition system.

4.3 Commissioning

The commissioning was initiated with a test to find gas leakages. The fluidization gas flows were set to 500Nl/min and water-soap spray was used to detect any leakages. Several leaks were detected from the seams at the loop-seals. These leaks were sealed after which no more leakages were found from the cold model.

The pressure differences over the distribution plates were measured at different fluidization volume flows. This was done to attain information of the pressure drop over the plates when they are clean. Also it verifies how calculated values differ from the measurements.

The air amplifier and possibility to adjust pressure at the risers were tested. The air amplifier gas pressure was adjusted and the change at absolute pressure was examined.

The bronze particles are weighted and inserted into the reactor system over the loop-seal. Bronze is fluidized evenly to both risers from the loop-seal. The addition of solids is stopped and the riser section which does not have a full loop-seal is fluidized. The solid circulates to another loop-

seal which gets filled. When both loop-seals are gas tight, more solid can be added and full recirculation of the first reactor can be started.

To keep the commissioning simple, first the smaller riser was set to the circulation mode. This means that only that part of the loop-seal exits were fluidized. A stable recirculation in the 40mm riser was obtained and pressure measurements were made. The fluidization of the smaller riser was gradually taken down and the same procedure was done to the 69mm riser.

After that both reactors were fluidized simultaneously, but the recirculation loops were separated. This means that the loop-seal after the reactor circulated solid material back to the same reactor. When stable fluidization was witnessed, this circulation was marked as achieved.

Step changes to the loop-seal fluidization were made. Fluidization changed from a recycle chamber to another at loop-seal which also changed the solid circulation from one reactor to another. Some instability at fluidization was observed which may be due to the step change in the process, or difference in the recycle chambers. Finally, a full recirculation of two interconnected fluidized beds with double loop-seal was obtained.

4.4 Preliminary fluidization tests

Preliminary fluidization tests were made to find stable fluidization conditions for both reactors and also to get a better idea how well double loop-seal works at different fluidization conditions.

The change in fluidization is studied using pressure and suspension density profiles which are calculated from the pressure difference measurements. In Fig. 9 to Fig. 16 the legend states the reactor, superficial velocity at the reactor and the loop-seal. Gas superficial velocity at reactor is presented after that which is calculated from the fluidization volume flow to reactor grate.

R1 refers to the 40mm reactor and R2 to the 69mm reactor. The loop-seals are presented as LSxRy, where x indicates the reactor where the solid comes to the loop-seal and y indicates the side where the solid

exits the loop-seal. For example, LS2R1 means that the solid comes from reactor 2 and is fluidized to reactor 1.

Fluidizations of the loop-seals are presented as the relation between the superficial velocities at recycle chamber and the calculated minimum fluidization velocity of the solid. This describes fluidization better than a simple superficial velocity of gas. Solid inventory is calculated from the pressure drop in the reactor riser.

In a preliminary run, fluidization changes were tested at the 40mm reactor to keep measurements simple. Data in the graphs below are from stable conditions and calculated from average pressures over 5 minutes. Red line at the height of 250mm corresponds to the location where the solids and gas from the loop-seals are introduced into reactor.

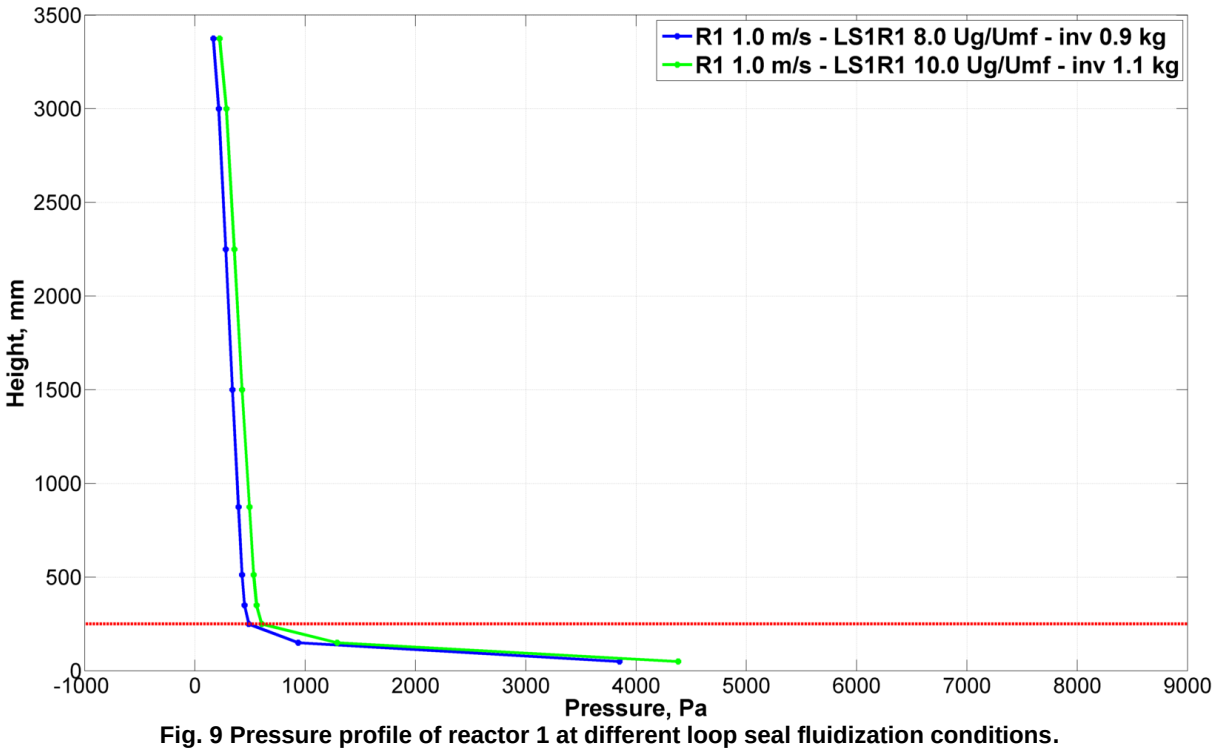

Fig. 9 Pressure profile of reactor 1 at different loop seal fluidization conditions.

Figures 9. and 10. present a case where fluidization at the loop-seal is increased. The graph shows that this increases the suspension density and therefore inventory at reactor 1, but the shape of the pressure profile stays similar. Note that the suspension density is higher than for sand due to the used bronze particles.

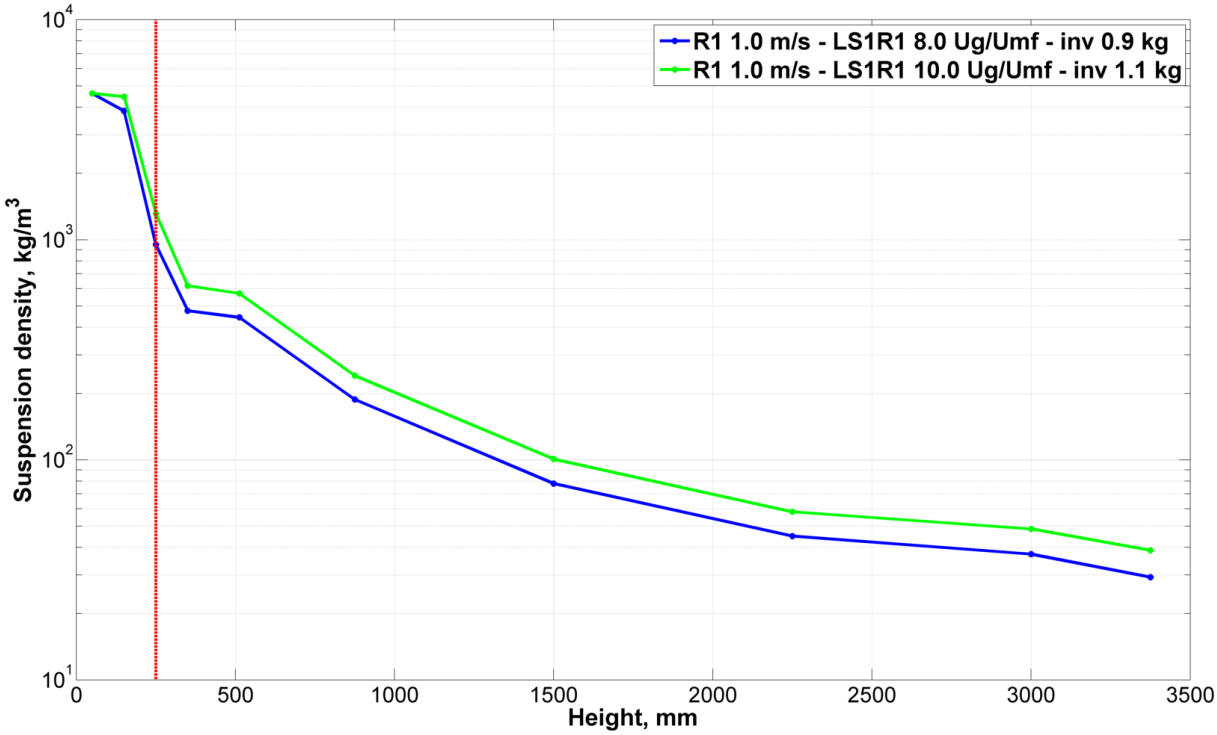

Fig. 10 Density profile of reactor 1 at different loop-seal fluidization conditions.

When the loop-seal fluidization has been constant but the reactor fluidization has been changed, the pressure profile changes, see Fig. 11. and Fig. 12.

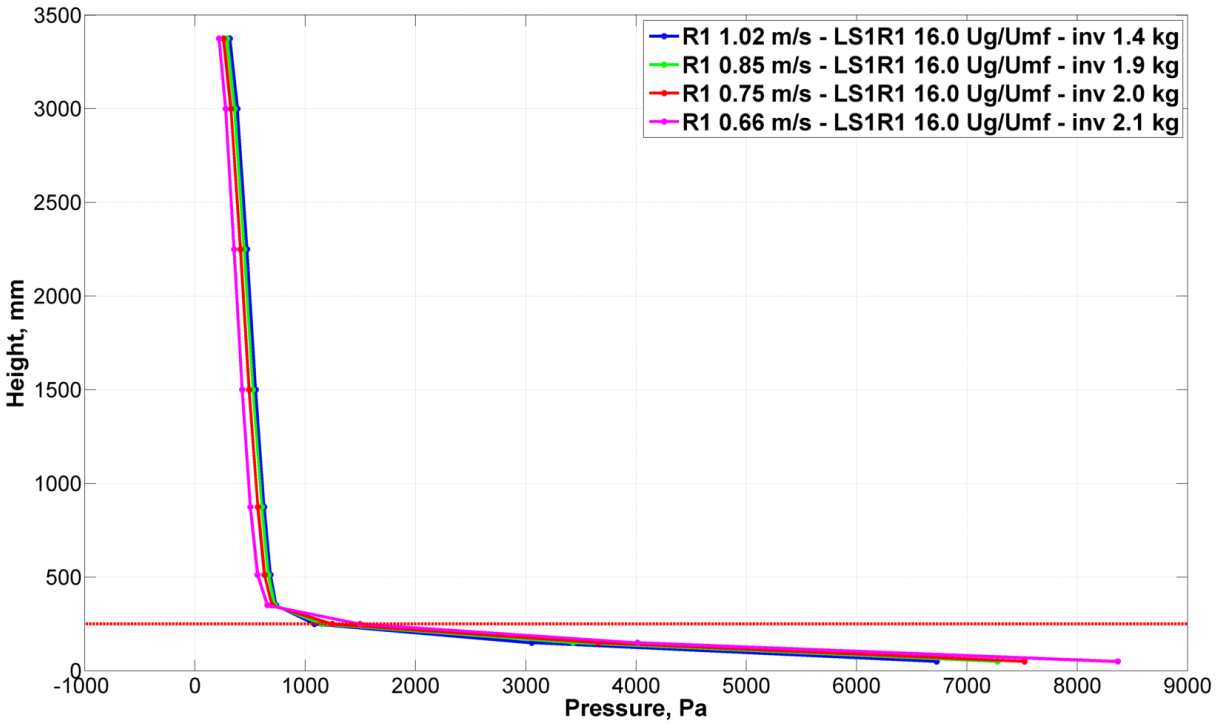

Fig. 11 Pressure profile of reactor 1 at different reactor fluidization conditions.

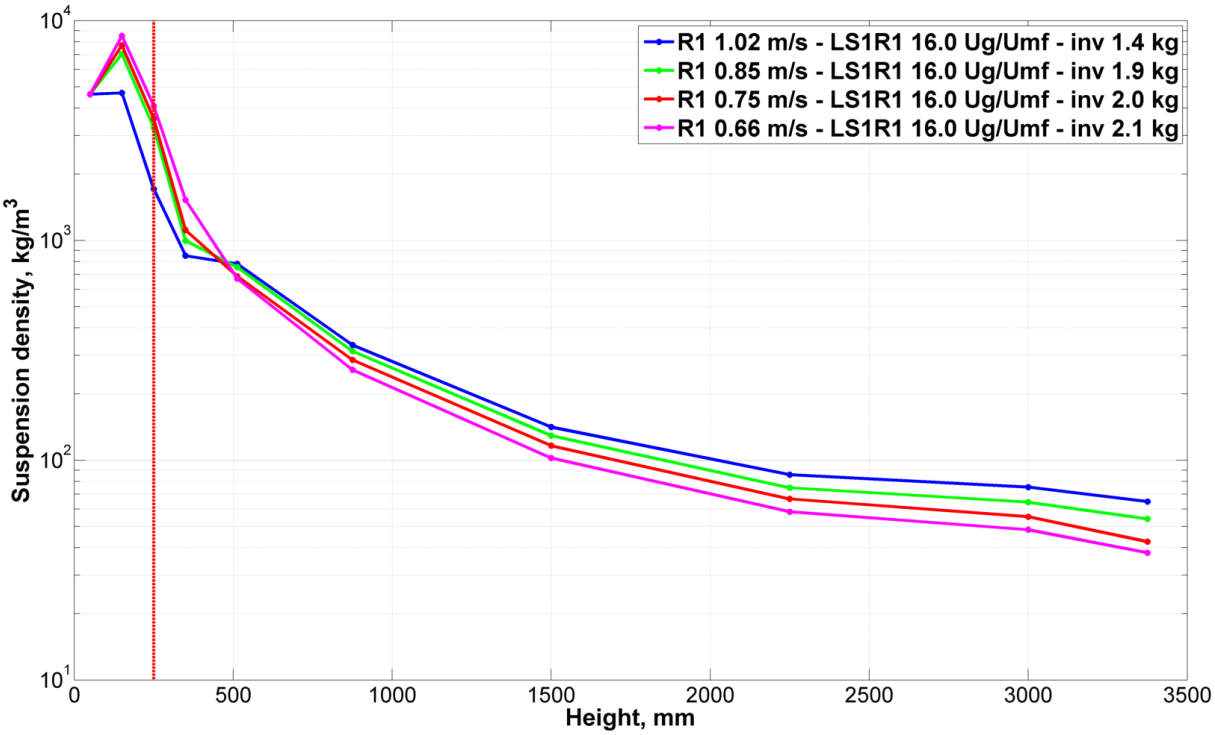

Fig. 12 Density profile of reactor 1 at different reactor fluidization conditions.

Fluidization at the reactor decreases below 250mm. This increases the density at the dense bed region. The profiles are also different above 500mm which also causes lower fluidization at the bottom. Fluidization at the bottom does not exceed the terminal velocity of the largest particles which are not carried to the top parts of the reactor. When fluidization at the bottom decreases, the pressure difference increases abnormally, the cause of this is still under investigation.

4.5 Fluidization tests and measurements

Fluidization tests with both reactors were made separately and in the interconnected mode. First both reactors were run separately at the same time, which means that both loop-seals returned the solids back to the same reactor.

These tests, see Fig. 13. and Fig. 14., were made to maintain stable conditions simultaneously in both reactors, to provide similar fluidization conditions in both reactors and to understand pressure handling over the double exit loop-seal.

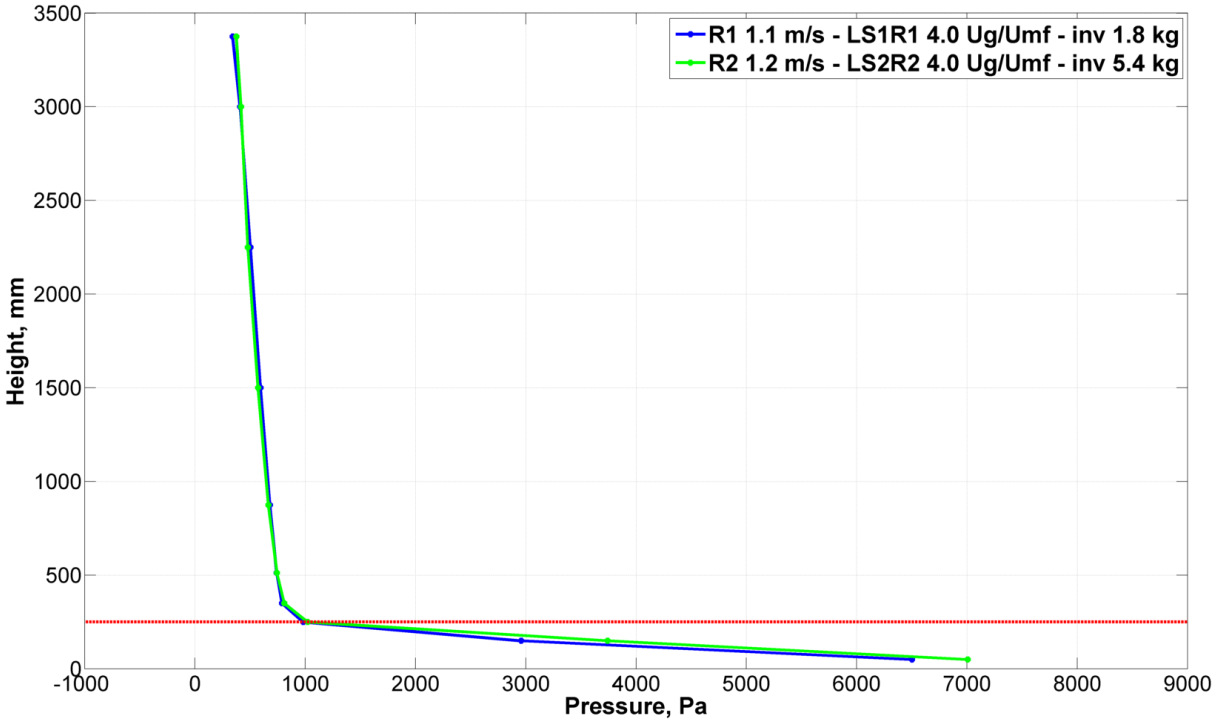

Fig. 13 Pressure profiles of both reactors at separated recirculation.

Both the pressure and density profiles are similar. Note that the inventory is different due to the different reactor size. The double exit loop-seal works well when the pressure on both sides of the exits is similar. This can be seen at height of 250mm where the pressure is similar at both reactors.

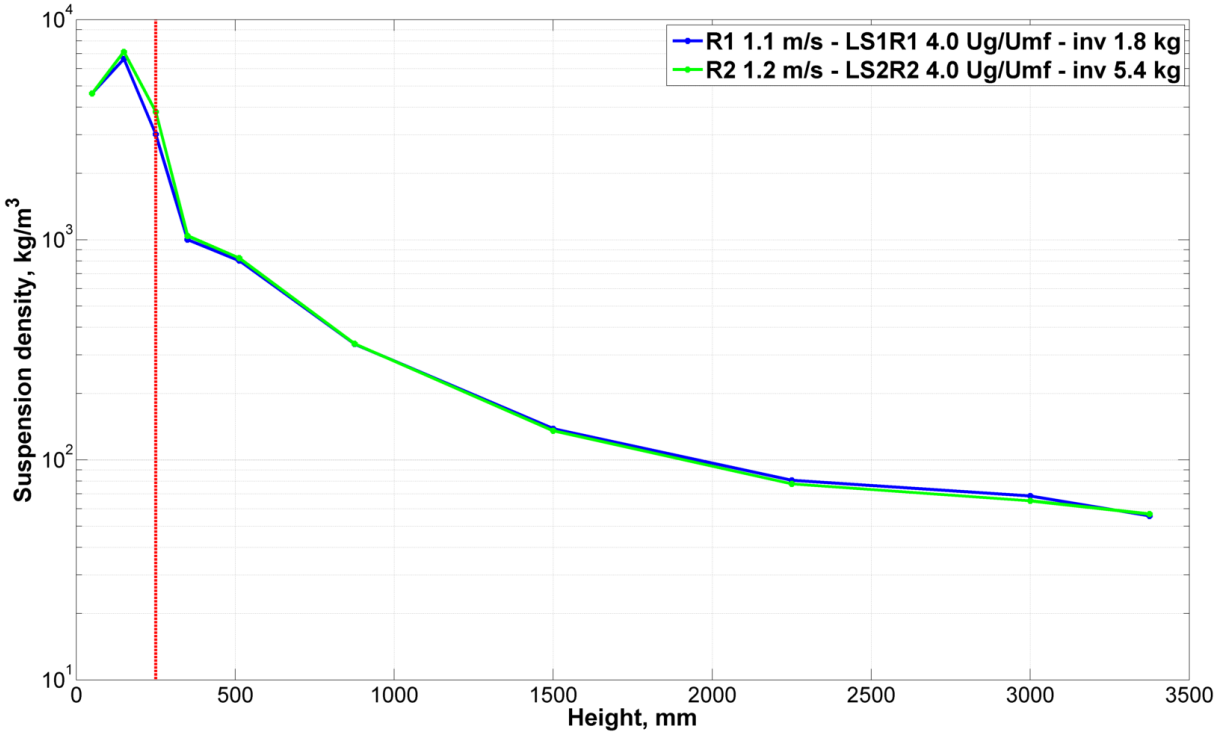

Fig. 14 Density profiles of both reactors at separated recirculation.

After separated recirculation, the loop-seal fluidization was changed. The reactors and loop-seals were interconnected and solid circulated between reactors. The resulting pressure and density profiles can be seen in Fig. 15. and Fig. 16.

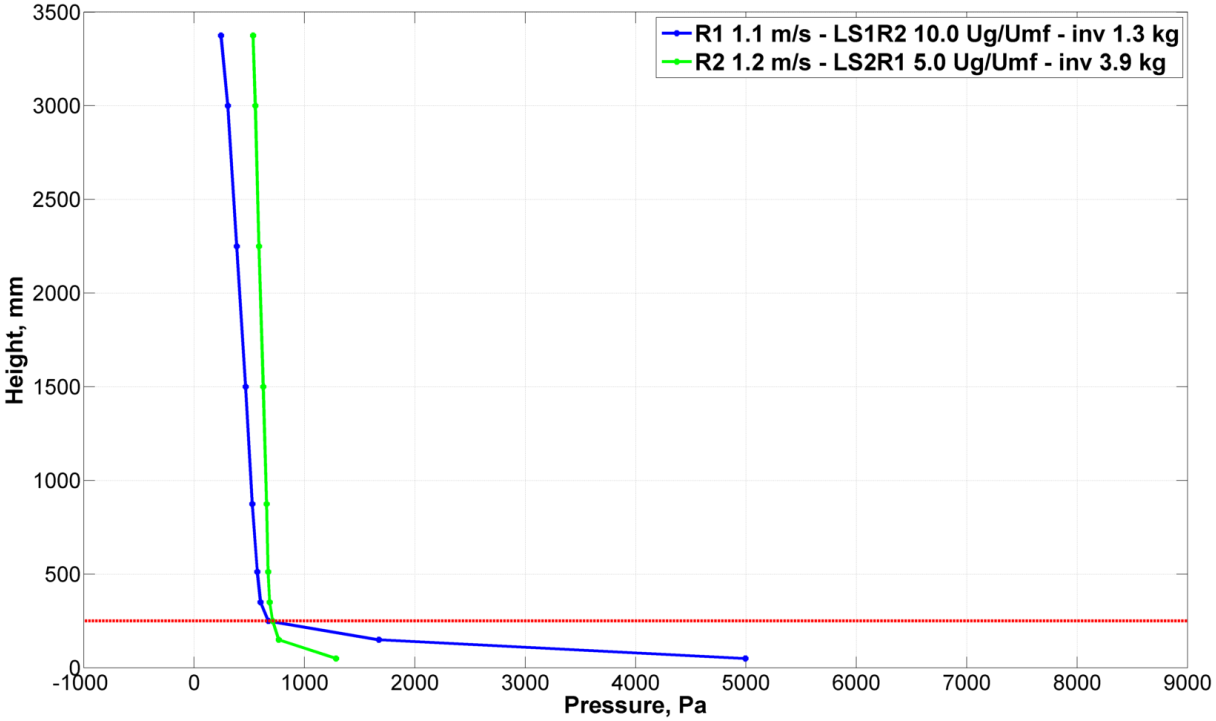

Fig. 15 Pressure profiles of both reactors at interconnected recirculation.

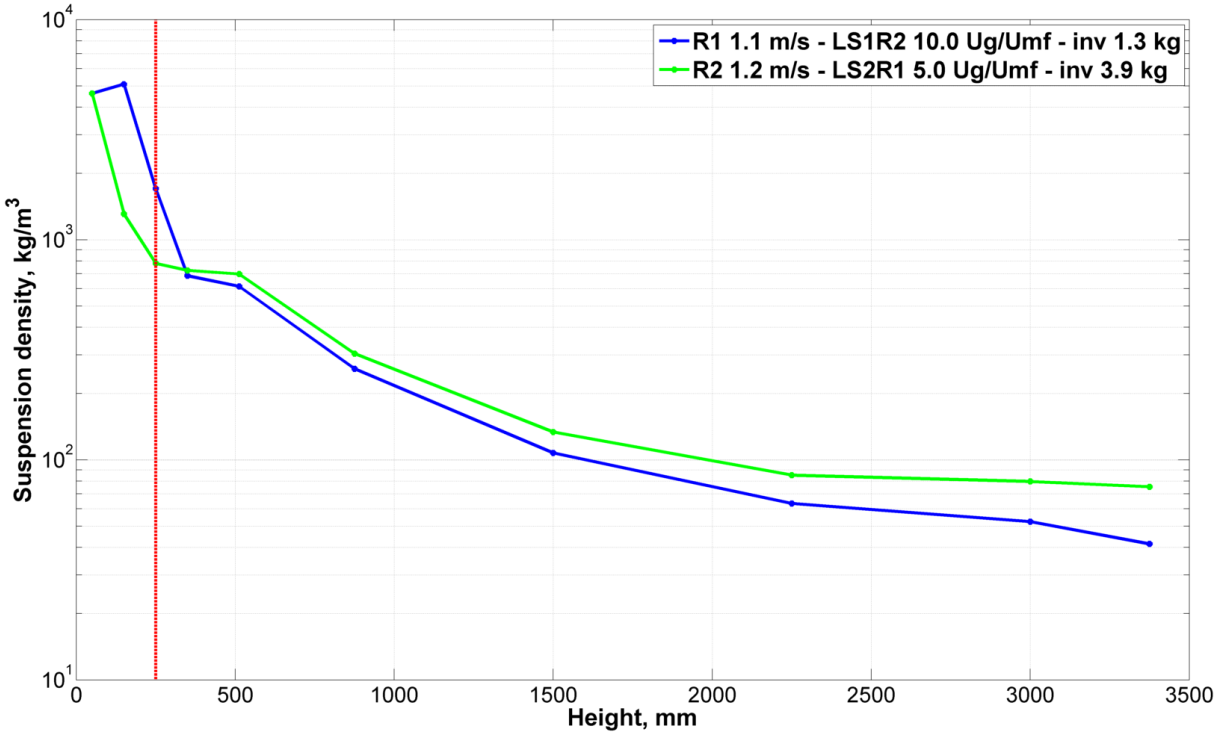

Fig. 16 Density profiles of both reactors at separated recirculation.

The importance of the requirement for pressure similarity between the loop-seal exits increases when the reactor system is in the interconnected mode. The pressure between reactors is adjusted to be similar at height of 250mm, which can be seen at Fig. 15.

Difficulty in the interconnected mode is to keep the fluidization from both loop-seals the same. If this is not successful, one loop-seal tends to empty and a gas leakage occurs. This can be prevented with measurements and control automation, a practical solution to this is under investigation.

During commissioning minor problems were encountered with gas leakages from the loop-seal seams. The primary cyclones could be smaller for the two smallest reactor sizes, 40mm and 69mm. The gas velocity in the cyclone increases when a larger reactor or higher fluidization velocity is used. Secondary cyclones still separate solids efficiently.

In these fluidization tests, all different connection modes were tested and stable conditions were achieved. It can be concluded that double exit loop-seals can be used to control solid flow, inventory and density profile at interconnected fluidized beds. Commissioning and fluidization test were successful.

5 References

Bi, H. T., Ellis, N., Abba, I. A. & Grace, J. R., 2000. A state-of-the-art review of gas-solid turbulent fluidization. *Chemical Engineering Science,* #nov#, 55table21), pp. 4789-4825.

Geldart, D., 1973. Types of gas fluidization. *Powder Technology,* #may#, 7(5), pp. 285-292.

Glicksman, L. R., 1984. Scaling relationships for fluidized beds. *Chemical Engineering Science,* 39(9), pp. 1373-1379.

Grace, J. R., 1986. Contacting modes and behaviour classification of gasâ€”solid and other two-phase suspensions. *Can. J. Chem. Eng.,* 64(3), pp. 353-363.

Johansson, A., Johnsson, F. & Leckner, B., 2007. Solids back-mixing in CFB boilers. *Chemical Engineering Science,* #jan#, 62(1â€“2), pp. 561-573.

Johansson, M., 2007. *Screening of oxygen-carrier particles based on iron-, manganese-, copper- and nickel oxides for use in chemical-looping technologies,* s.l.: s.n.

Kunii, D. & Levenspiel, O., 1977. *Fluidization engineering.* s.l.:Robert E. Krieger Publishing Company, Inc..

Raiko, R., Kurki-Suonio, I., Saastamoinen, J. & Hupa, M. e., 2002. *Poltto ja palaminen.* s.l.:International Flame Research Foundation - Suomen kansallinen osasto.

Schmid, J. et al., 2011. *A new dual fluidized bed gasifier design for improved in situ conversion of hydrocarbons.* s.l., s.n.

Yang, W.-C., 2003. *Handbook of fluidization and fluid-particle systems.* s.l.:CRC Press.